

**Douglas Ollerenshaw**  
Graduate Research Assistant  
Department of Mechanical Engineering,  
Oregon State University,  
Corvallis, OR 97331

**Mark Costello**  
Associate Professor  
Mem. ASME  
School of Aerospace Engineering,  
Georgia Institute Of Technology,  
Atlanta, GA 30327

# Model Predictive Control of a Direct Fire Projectile Equipped With Canards

*Launch uncertainties in uncontrolled direct fire projectiles can lead to significant impact point dispersion, even at relatively short range. A model predictive control scheme for direct fire projectiles is investigated to reduce impact point dispersion. The control law depends on projectile linear theory to create an approximate linear model of the projectile and quickly predict states into the future. Control inputs are based on minimization of the error between predicted projectile states and a desired trajectory leading to the target. Through simulation, the control law is shown to work well in reducing projectile impact point dispersion. Parametric trade studies on an example projectile configuration are reported that detail the effect of prediction horizon length, gain settings, model update interval, and model step size. [DOI: 10.1115/1.2957624]*

## Introduction

Direct fire projectiles are fired by line-of-sight aiming and are fired from ground based platforms, helicopters, and fixed wing aircraft. A number of conditions can cause rounds to miss an intended target. These conditions include manufacturing inaccuracies of the gun tube, propellant, and projectile, along with variable atmospheric conditions, firing platform motion, and aiming errors. With the advent of low cost, small, rugged, microelectromechanical systems, dramatic reduction in dispersion for direct fire projectiles equipped with a relatively inexpensive flight control system is possible. One design concept consists of a set of controllable canards located near the nose of the projectile. This paper develops a unique flight control law tailored to control of smart projectiles through the application of model predictive control (MPC) and projectile linear theory.

In model predictive control, a dynamic model of the plant is used to project the state into the future and subsequently use the estimated future state to determine control action. It has been found to be a practical and increasingly employed control technique [1]. Currently, model predictive control is being applied to a wide variety of problems, spanning many different industries. Mei et al. [2] studied vibration reduction in a tall building experiencing wind excitation using model predictive control and linear quadratic gaussian control strategies. They found that the model predictive control scheme performed well and was robust to uncertainty in building stiffness. Tsai and Huang [3] used a model reference adaptive predictive controller for a variable-frequency oil-cooling machine used in concert with dynamically complex machine tools. Kvaternik et al. [4] developed a generalized predictive controller for tiltrotor aeroelastic stability augmentation in airplane mode of flight. Using the model predictive control strategy, significant increases in damping of aircraft body vibration modes were achieved in a wind tunnel test. Slegers and Costello [5] applied model predictive control to a parafoil for autonomous delivery of a payload in battlefield conditions. Burchett and Costello [6] used a simplified form of model predictive control applied to a projectile with lateral pulse jets. Their strategy was to use projectile linear theory to map the projected impact point in the vertical target plane and base control action on projected miss distance and direction. The key difference between their strategy

and that detailed here is that the control strategy employed by Burchett and Costello calculated errors only in the target plane, while the control strategy used here considers error along the length of the trajectory. In addition, the pulse jet control scheme used by Burchett and Costello is inherently discontinuous and can only be applied at a discrete number of points. Canard control, as applied in this paper, is continuous and is applied for the full flight duration.

Any model predictive control scheme is dependent on the accuracy of the underlying dynamic model representing the plant. Under most flight conditions, the equations of motion for a projectile in atmospheric flight can be adequately represented by a six degree of freedom rigid body model with externally applied aerodynamic forces and moments. The resulting differential equations have been shown to provide an accurate representation of projectile flight characteristics [7], though their inherent nonlinearity prevents direct use in model predictive control applications. However, a series of manipulations and simplifications of the equations of motion allows closed form solution of the projectile trajectory under restricted flight conditions. The simplified dynamic equations and their resulting solutions have become known as projectile linear theory. Projectile linear theory has been extended by various authors to handle more sophisticated aerodynamic models [8], asymmetric mass properties [9], fluid payloads [10,11], moving internal parts [12,13], dual spin projectiles [14,15], ascending flight [16], and lateral force impulses [17–20]. Aerodynamic range reduction software used in spark range facilities utilizes projectile linear theory in estimation of aerodynamic coefficients.

The work reported below employs model predictive control and projectile linear theory for control of a direct fire projectile. The basic projectile configuration under consideration is fin stabilized and the fins are slightly canted to provide moderate roll rates during flight. A set of controllable canards located near the nose of the projectile is used as the control mechanism. The canards can be directed to provide swerve forces and pitch and yaw moments to the projectile. The control law uses an approximate closed form solution of projectile motion to predict the states of the projectile over a set distance known as the prediction horizon. Current and future control actions are determined based on minimizing the estimated error of future states. It is assumed that sensor feedback is provided by an onboard inertial measurement unit (IMU).

Simulation results to establish the utility of the new model predictive flight control system design methodology are generated for an exemplar projectile. All control system calculations are performed in separate subroutines to mimic the calculations, which would be performed using a projectile onboard processor. The

Contributed by the Dynamic Systems, Measurement, and Control Division of ASME for publication in the JOURNAL OF DYNAMIC SYSTEMS, MEASUREMENT, AND CONTROL. Manuscript received September 12, 2004; final manuscript received March 13, 2008; published online October 1, 2008. Assoc. Editor Atul Kelkar.

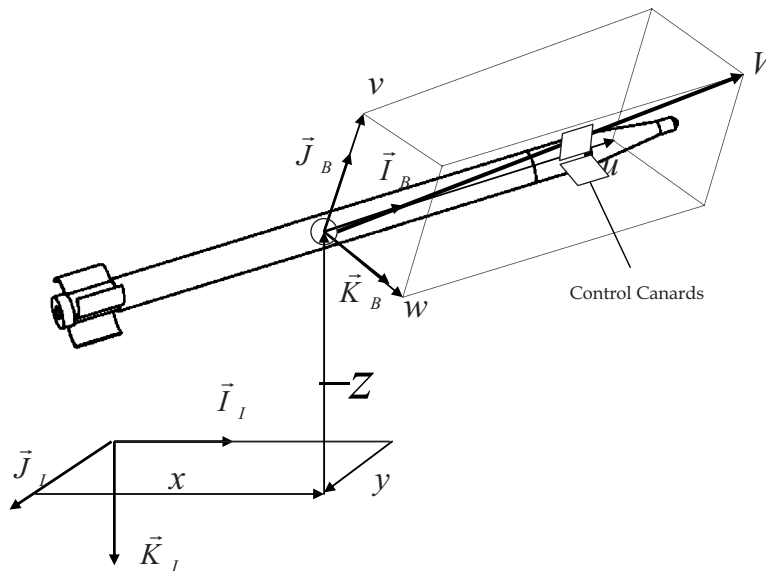


Fig. 1 Schematic of the position coordinates of a direct fire projectile

inputs to the control system subroutines are simulated sensor feedback signals. The outputs of the control subroutines are the control commands, which, in a physical application, would be sent directly to the control actuators. In the code, these control commands are applied to a fully nonlinear six degree of freedom dynamic model of a projectile. The nonlinear dynamic model uses mass and inertia properties and aerodynamic coefficient lookup tables specific to the projectile being studied. Parametric trade studies are conducted that consider the effect on impact point dispersion caused by modifying various control system properties. The control system properties examined are the cost function weighting matrices, prediction horizon length, state estimation

step size, and the linear model update interval.

### Projectile Dynamic Model

The nonlinear trajectory simulation used in this study is a standard six degree of freedom model typically used in flight dynamic modeling of projectiles. A schematic of the projectile configuration is shown in Figs. 1 and 2. The six degrees of freedom are the three inertial components of the position vector from an inertial frame to the projectile mass center and the three standard Euler orientation angles. The equations of motion are provided in Eqs. (1)–(4) [21–23]

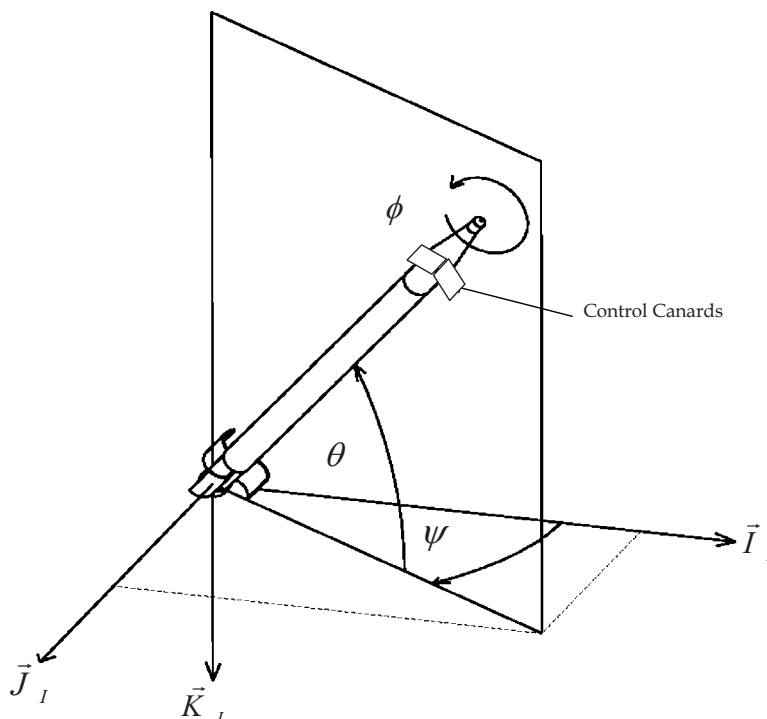


Fig. 2 Schematic of the attitude coordinates of a direct fire projectile

$$\begin{Bmatrix} \dot{x} \\ \dot{y} \\ \dot{z} \end{Bmatrix} = \begin{bmatrix} c_{\theta}c_{\psi} & s_{\phi}s_{\theta}c_{\psi} - c_{\phi}s_{\psi} & c_{\phi}s_{\theta}c_{\psi} + s_{\phi}s_{\psi} \\ c_{\theta}s_{\psi} & s_{\phi}s_{\theta}s_{\psi} + c_{\phi}c_{\psi} & c_{\phi}s_{\theta}s_{\psi} - s_{\phi}c_{\psi} \\ -s_{\theta} & s_{\phi}c_{\theta} & c_{\phi}c_{\theta} \end{bmatrix} \begin{Bmatrix} u \\ v \\ w \end{Bmatrix} \quad (1)$$

$$\begin{Bmatrix} \dot{\phi} \\ \dot{\theta} \\ \dot{\psi} \end{Bmatrix} = \begin{bmatrix} 1 & s_{\phi}t_{\theta} & c_{\phi}t_{\theta} \\ 0 & c_{\phi} & -s_{\phi} \\ 0 & s_{\phi}/c_{\theta} & c_{\phi}/c_{\theta} \end{bmatrix} \begin{Bmatrix} p \\ q \\ r \end{Bmatrix} \quad (2)$$

$$\begin{Bmatrix} \dot{u} \\ \dot{v} \\ \dot{w} \end{Bmatrix} = \begin{Bmatrix} X/m \\ Y/m \\ Z/m \end{Bmatrix} - \begin{bmatrix} 0 & -r & q \\ r & 0 & -p \\ -q & p & 0 \end{bmatrix} \begin{Bmatrix} u \\ v \\ w \end{Bmatrix} \quad (3)$$

$$\begin{Bmatrix} \dot{p} \\ \dot{q} \\ \dot{r} \end{Bmatrix} = [I]^{-1} \begin{bmatrix} L \\ M \\ N \end{bmatrix} - \begin{bmatrix} 0 & -r & q \\ r & 0 & -p \\ -q & p & 0 \end{bmatrix} \begin{Bmatrix} p \\ q \\ r \end{Bmatrix} \quad (4)$$

In Eqs. (1) and (2), the standard shorthand notation for trigonometric functions is used:  $\sin(\alpha) \equiv s_{\alpha}$ ,  $\cos(\alpha) \equiv c_{\alpha}$ , and  $\tan(\alpha) \equiv t_{\alpha}$ . The forces appearing in Eq. (3) contain contributions from weight ( $W$ ), body aerodynamics ( $A$ ), and the control canards ( $C$ ).

$$\begin{Bmatrix} X \\ Y \\ Z \end{Bmatrix} = \begin{Bmatrix} X_W \\ Y_W \\ Z_W \end{Bmatrix} + \begin{Bmatrix} X_A \\ Y_A \\ Z_A \end{Bmatrix} + \begin{Bmatrix} X_C \\ Y_C \\ Z_C \end{Bmatrix} \quad (5)$$

The dynamic equations are expressed in a body fixed reference frame; thus all forces acting on the body are expressed in the projectile reference frame. The weight force is shown in Eq. (6),

$$\begin{Bmatrix} X_W \\ Y_W \\ Z_W \end{Bmatrix} = mg \begin{Bmatrix} -s_{\theta} \\ s_{\phi}c_{\theta} \\ c_{\phi}c_{\theta} \end{Bmatrix} \quad (6)$$

while the aerodynamic force acting at the center of pressure of the projectile is given by Eq. (7).

$$\begin{Bmatrix} X_A \\ Y_A \\ Z_A \end{Bmatrix} = -\frac{\pi}{8}\rho V^2 D^2 \begin{Bmatrix} C_{X0} + C_{X2}(v^2 + w^2)/V^2 \\ C_{NA}v/V \\ C_{NA}w/V \end{Bmatrix} \quad (7)$$

The control forces are the aerodynamic drag forces created by the control canards in the directions perpendicular to the axis of symmetry of the projectile.

$$\begin{Bmatrix} X_C \\ Y_C \\ Z_C \end{Bmatrix} = -\frac{\pi}{8}\rho V^2 D^2 \begin{Bmatrix} 0 \\ C_{Y0} \\ C_{Z0} \end{Bmatrix} \quad (8)$$

The applied moments about the projectile mass center contain contributions from steady aerodynamics (SA), unsteady aerodynamics (UA), and the control canards ( $C$ ).

$$\begin{Bmatrix} L \\ M \\ N \end{Bmatrix} = \begin{Bmatrix} L_{SA} \\ M_{SA} \\ N_{SA} \end{Bmatrix} + \begin{Bmatrix} L_{UA} \\ M_{UA} \\ N_{UA} \end{Bmatrix} + \begin{Bmatrix} L_C \\ M_C \\ N_C \end{Bmatrix} \quad (9)$$

The moment components due to steady aerodynamic forces and control canard forces are computed with a cross product between the distance vector from the mass center to the location of the specific force and the force itself. The unsteady body aerodynamic moment provides a damping source for projectile angular motion and is given by Eq. (9).

$$\begin{Bmatrix} L_{UA} \\ M_{UA} \\ N_{UA} \end{Bmatrix} = \frac{\pi}{8}\rho V^2 D^3 \begin{Bmatrix} C_{DD} + \frac{pDC_{LP}}{2V} \\ \frac{qDC_{MQ}}{2V} \\ \frac{rDC_{MQ}}{2V} \end{Bmatrix} \quad (10)$$

The mass, mass center location, and inertial properties of the projectile are all assumed to be constant throughout the duration of the flight. The center of pressure location and all aerodynamic coefficients ( $C_{X0}, C_{YPA}, C_{NA}, C_{DD}, C_{LP}, C_{MQ}$ ) depend on local Mach number and are computed during simulation using linear interpolation.

The dynamic equations given by Eqs. (1)–(4) are numerically integrated forward in time using a fourth order, fixed step Runge–Kutta algorithm. Costello and Anderson [7] present correlation of this dynamic model against range data for a fin stabilized projectile.

### Projectile Linear Theory Trajectory Solution

The six degree of freedom rigid body projectile model shown above consists of 12 highly nonlinear differential equations for which a closed form solution has not been directly found. Significant work has been performed to simplify the equations of motion such that an accurate analytical solution can be determined. In order to arrive at a set of analytically solvable ordinary linear differential equations, the following assumptions and simplifications are made:

- (1) Rather than employing a reference frame fixed to the projectile body, projectile linear theory uses an intermediate reference frame, which is aligned with the projectile axis of symmetry but does not roll. Lateral translational and rotational velocity components described in this frame, known as the no-roll frame or the fixed plane frame, are denoted with a  $\sim$  superscript. Components of the linear and angular body velocities in the fixed plane frame are computed from body frame components of the same vector through a single axis rotation transformation. For example, the body frame components of the projectile mass center velocity are transformed to the fixed plane by

$$\begin{Bmatrix} \tilde{u} \\ \tilde{v} \\ \tilde{w} \end{Bmatrix} = \begin{bmatrix} 1 & 0 & 0 \\ 0 & c_{\phi} & -s_{\phi} \\ 0 & s_{\phi} & c_{\phi} \end{bmatrix} \begin{Bmatrix} u \\ v \\ w \end{Bmatrix} \quad (11)$$

- (2) A change of variables is made from the velocity along the projectile axis of symmetry,  $u$ , to the total velocity,  $V$ . Equations (11) and (12) relate  $V$  and  $u$  and their derivatives.

$$V = \sqrt{u^2 + v^2 + w^2} = \sqrt{u^2 + \tilde{v}^2 + \tilde{w}^2} \quad (12)$$

$$\dot{V} = \frac{u\dot{u} + v\dot{v} + w\dot{w}}{V} = \frac{u\dot{u} + \tilde{v}\dot{\tilde{v}} + \tilde{w}\dot{\tilde{w}}}{V} \quad (13)$$

- (3) Dimensionless arc length,  $s$ , is used as the independent variable instead of time,  $t$ . Equation (13) defines dimensionless arc length.

$$s = \frac{1}{D} \int_0^t V dt \quad (14)$$

Equations (14) and (15) relate time and arc length derivatives of a dummy variable  $\zeta$ . Dotted terms refer to time derivatives and primed terms denote arc length derivatives:

$$\dot{\zeta} = \left(\frac{V}{D}\right)\zeta' \quad (15)$$

$$\ddot{\xi} = \left(\frac{V}{D}\right)^2 \left(\xi'' + \frac{\xi' V'}{V}\right) \quad (16)$$

(4) Euler pitch and yaw angles are assumed to be small so that

$$\begin{aligned} \sin(\theta) &\approx \theta, & \cos(\theta) &\approx 1 \\ \sin(\psi) &\approx \psi, & \cos(\psi) &\approx 1 \end{aligned} \quad (17)$$

(5) Aerodynamic angles of attack are small so that

$$\alpha \approx \frac{w}{V}, \quad \beta \approx \frac{v}{V} \quad (18)$$

(6) The projectile is mass balanced such that the center of gravity lies in the rotational axis of symmetry:

$$\begin{aligned} I_{xy} &= I_{xz} = I_{yz} = 0 \\ I_R &= I_{xx} \\ I_P &= I_{yy} = I_{zz} \end{aligned} \quad (19)$$

(7) Quantities  $V$  and  $\phi$  are large compared to  $\theta, \psi, v, w, q,$  and  $r$  such that products of small quantities and their derivatives are negligible.

A more detailed discussion of the development of projectile linear theory is provided by McCoy [21]. Application of the above stated assumptions leads to a set of coupled linear differential equations, with the exception that the total velocity,  $V$ , the roll rate,  $p$ , and the pitch angle,  $\theta$ , appear in nonlinear fashion in many of the equations. To remedy this, the assumption is made that  $V$  changes slowly with respect to the other variables and is thus considered to be constant,  $V=V_0$ , when it appears as a coefficient in all dynamic equations except its own. In addition, the roll rate and pitch angle are held constant,  $p=p_0$  and  $\theta=\theta_0$ , only when they appear in nonlinear fashion. The equation for the total velocity is shown in Eq. (17).

$$V' = \frac{-\pi\rho D^3 C_{X0}}{8m} V - \frac{DgS_{\theta_0}}{V} \quad (20)$$

The remaining 11 equations can be written as

$$\begin{pmatrix} \tilde{v}' \\ \tilde{w}' \\ \tilde{q}' \\ \tilde{r}' \\ x' \\ y' \\ z' \\ \phi' \\ \theta' \\ \psi' \\ p' \end{pmatrix} = \begin{bmatrix} -A & 0 & 0 & -D & 0 & 0 & 0 & 0 & 0 & 0 & 0 \\ 0 & -A & D & 0 & 0 & 0 & 0 & 0 & 0 & 0 & 0 \\ B/D & C/D & H & -F & 0 & 0 & 0 & 0 & 0 & 0 & 0 \\ -C/D & B/D & F & H & 0 & 0 & 0 & 0 & 0 & 0 & 0 \\ 0 & 0 & 0 & 0 & 0 & 0 & 0 & 0 & 0 & 0 & 0 \\ D/V_0 & 0 & 0 & 0 & 0 & 0 & 0 & 0 & 0 & D & 0 \\ 0 & D/V_0 & 0 & 0 & 0 & 0 & 0 & 0 & -D & 0 & 0 \\ 0 & 0 & 0 & 0 & 0 & 0 & 0 & 0 & 0 & 0 & D/V_0 \\ 0 & 0 & D/V_0 & 0 & 0 & 0 & 0 & 0 & 0 & 0 & 0 \\ 0 & 0 & 0 & D/V_0 & 0 & 0 & 0 & 0 & 0 & 0 & 0 \\ 0 & 0 & 0 & 0 & 0 & 0 & 0 & 0 & 0 & 0 & K_c \end{bmatrix} \begin{pmatrix} \tilde{v} \\ \tilde{w} \\ \tilde{q} \\ \tilde{r} \\ x \\ y \\ z \\ \phi \\ \theta \\ \psi \\ p \end{pmatrix} + \begin{pmatrix} V_F \\ W_F \\ Q_F \\ R_F \\ D \\ 0 \\ 0 \\ 0 \\ 0 \\ 0 \\ P_F \end{pmatrix} \quad (21)$$

where

$$A = \frac{\pi\rho D^3 C_{NA}}{8m} \quad (22)$$

$$B = \frac{\pi\rho D^5 C_{YPA} p_0 \Delta SL_m}{16I_P V_0} \quad (23)$$

$$C = \frac{\pi\rho D^4 C_{NA} \Delta SL}{8I_P} \quad (24)$$

$$F = \frac{I_R D p_0}{I_P V_0} \quad (25)$$

$$H = \frac{\pi\rho D^5 C_{MQ}}{16I_P} \quad (26)$$

$$K_c = \frac{\pi\rho D^5 C_{LP}}{16I_R} \quad (27)$$

$$V_F = \frac{\pi\rho D^3}{8m} (C_{NA} \tilde{v}_* - V_0 C_{Y0}) \quad (28)$$

$$W_F = \frac{gDC_{\theta_0}}{V_0} + \frac{\pi\rho D^3}{8m} (C_{NA} \tilde{w}_* - V_0 C_{Z0}) \quad (29)$$

$$Q_F = \frac{\pi\rho D^3}{8I_P} \left( -\tilde{w}_* C_{NA} \Delta SL - \frac{DC_{YPA} p_0 \Delta SL_m \tilde{v}_*}{2V_0} + V_0 C_{Z0} \Delta SL_C \right) \quad (30)$$

$$R_F = \frac{\pi\rho D^3}{8I_P} \left( -\tilde{v}_* C_{NA} \Delta SL - \frac{DC_{YPA} p_0 \Delta SL_m \tilde{w}_*}{2V_0} - V_0 C_{Y0} \Delta SL_C \right) \quad (31)$$

$$P_F = \frac{\pi\rho V_0 D^4 C_{DD}}{8I_R} \quad (32)$$

Closed form solutions to the above equations can be found, though the results are omitted here. A more detailed treatment of the solutions to the projectile linear theory equations can be found in Ref. [23].

The variables  $C_{Y0}$  and  $C_{Z0}$  are aerodynamic trim forces perpendicular to the projectile axis of symmetry, which are created by movement of the control canards and are treated directly as control inputs.

In reality, the total velocity,  $V$ , does not remain constant for the duration of the flight. Therefore, the total velocity must be peri-

odically measured throughout the trajectory and updated in the remaining equations. The center of pressure location and the aerodynamic coefficients ( $C_{X0}$ ,  $C_{YPA}$ ,  $C_{NA}$ ,  $C_{DD}$ ,  $C_{LP}$ , and  $C_{MQ}$ ), which all depend on local Mach number, must also be recomputed each time  $V$  is updated. The effect of the length of the update interval on the accuracy of the model was studied by Burchett et al. [19].

### Model Predictive Flight Control System

The model predictive controller uses the linearized model of the system to propagate the states forward in time over an interval known as the prediction horizon ( $H_p$ ) [24]. Control action is based on comparison of the predicted states and a predetermined desired trajectory over the prediction horizon. As the prediction step is marched forward, so too is the prediction horizon; a process referred to as the "receding horizon principle." The control action at each step is determined by minimizing a quadratic cost function defined as

$$J = (W - \tilde{Y})^T Q (W - \tilde{Y}) + U^T R U \quad (33)$$

The matrix  $W$  contains the desired system outputs,  $w$ , over the length of the prediction horizon. The desired system outputs,  $w$ , at each prediction step consists of the desired  $x$ ,  $y$ , and  $z$  coordinates at that time instant. These values need to be loaded into the on-board computer prior to projectile launch.

$$W = \begin{Bmatrix} w_{k+1} \\ w_{k+2} \\ \vdots \\ w_{k+H_p} \end{Bmatrix}, \quad w_{k+i} = \begin{Bmatrix} x_{k+i} \\ y_{k+i} \\ z_{k+i} \end{Bmatrix} \quad (34)$$

The matrix  $\tilde{Y}$  contains the predicted system outputs,  $\tilde{y}$ , and the matrix  $U$  contains the calculated system inputs,  $u$ , as follows:

$$\tilde{Y} = \begin{Bmatrix} \tilde{y}_{k+1} \\ \tilde{y}_{k+2} \\ \vdots \\ \tilde{y}_{k+H_p} \end{Bmatrix}, \quad U = \begin{Bmatrix} u_k \\ u_{k+1} \\ \vdots \\ u_{k+H_p-1} \end{Bmatrix} \quad (35)$$

$Q$  and  $R$  are diagonal positive semidefinite weighting matrices.

In order to develop an expression for the predicted system outputs over the prediction horizon, the system is first cast in standard discrete state-space form

$$\begin{aligned} x_{k+1} &= A(\Delta s)x_k + B(\Delta s)u_k + F(\Delta s) \\ y_k &= Cx_k \end{aligned} \quad (36)$$

where the values within the matrices  $A$ ,  $B$ , and  $F$ , depend on the arc length step size ( $\Delta s$ ). The projectile linear theory expressions shown in the previous section are used to form the state-space matrices through a 14-step loop in the control algorithm. In the first step, all of the states and controls are set to zero and the solutions are evaluated over one arc length step to determine the values within the constant vector,  $F$ . In the next step, the first state,  $\tilde{w}$ , is set equal to 1, with the remaining states and controls still equal to zero, and the expressions are reevaluated. By subtracting the values of the constants,  $F$ , the coefficients making up the first column of  $A$  can be found. This process, consisting of setting a state variable equal to 1, evaluating the linear theory solutions, then subtracting the constant values, is repeated for each of the remaining ten states to fully populate the state matrix  $A$  one column at a time. The control matrix,  $B$ , is formed in exactly the same manner with all 11 states equal to zero and the controls,  $C_{Y0}$  and  $C_{Z0}$ , alternately set equal to 1.

The desired outputs of the system are its center of mass position states ( $x$ ,  $y$ , and  $z$ ). The matrix  $C$  is then simply

$$C = \begin{bmatrix} 0 & 0 & 0 & 0 & 1 & 0 & 0 & 0 & 0 & 0 & 0 \\ 0 & 0 & 0 & 0 & 0 & 1 & 0 & 0 & 0 & 0 & 0 \\ 0 & 0 & 0 & 0 & 0 & 0 & 1 & 0 & 0 & 0 & 0 \end{bmatrix} \quad (37)$$

A recursive formula can be found for  $y_{k+j}$ ,  $1 \leq j \leq H_p$  by substituting the expression for  $x_{k+j}$  into the expression for  $y_{k+j}$ . The result is

$$y_{k+j} = CA^j x_k + \sum_{i=1}^j CA^{j-i} B u_{k+i-1} + \sum_{i=1}^j CA^{j-i} F \quad (38)$$

or in matrix form

$$\tilde{Y} = K_{CA} x_k + K_{CAB} U + K_{CAF} \quad (39)$$

where

$$K_{CA} = \begin{bmatrix} CA \\ CA^2 \\ CA^3 \\ \vdots \\ CA^{H_p} \end{bmatrix} \quad (40)$$

$$K_{CAB} = \begin{bmatrix} CB & 0 & 0 & \dots & 0 \\ CAB & CB & 0 & \dots & \vdots \\ CA^2 B & CAB & CB & \dots & 0 \\ \vdots & \vdots & \vdots & \ddots & 0 \\ CA^{H_p-1} & \dots & CA^2 B & CAB & CB \end{bmatrix} \quad (41)$$

$$K_{CAF} = \begin{bmatrix} CF \\ CAF + CF \\ CA^2 F + CAF + CF \\ \vdots \\ CA^{H_p-1} F + \dots + CAF + CF \end{bmatrix} \quad (42)$$

The cost function,  $J$ , then becomes

$$J = (W - K_{CA} x_k - K_{CAB} U - K_{CAF})^T Q (W - K_{CA} x_k - K_{CAB} U - K_{CAF}) + U^T R U \quad (43)$$

The minimum of the cost function is determined by selecting the control input vector that forces the gradient of the cost function to zero.

$$U = K(W - K_{CA} x_k - K_{CAF}) \quad (44)$$

where

$$K = (K_{CAB}^T Q K_{CAB} + R)^{-1} K_{CAB}^T Q \quad (45)$$

It should be noted that  $U$  contains the optimal control inputs over the entire prediction horizon. At each arc length step,  $k$ , only  $u_k$  is used, which is the first element of  $U$ . The first element of  $U$  is

$$u_k = K_1 (W - K_{CA} x_k - K_{CAF}) \quad (46)$$

where  $K_1$  consists only of the first  $M$  rows of  $K$ . Note that  $M$  is defined as the number of control inputs, which, in this application, is 2 ( $C_{Y0}$  and  $C_{Z0}$ ).

It is assumed that full state feedback is available for use in the control law, that is  $x$ ,  $y$ ,  $z$ ,  $\psi$ ,  $\theta$ ,  $\phi$ ,  $u$ ,  $v$ ,  $w$ ,  $p$ ,  $q$ , and  $r$  are sensed or estimated by the IMU. Furthermore, the weapon that fires the projectile provides a desired trajectory leading to the target. At time=0, the controller is provided with the full state of the projectile. The total velocity,  $V$ , is calculated from the projectile mass center velocity states and set to  $V_0$  in the linear model. The linear model is then used to propagate the remaining 11 states forward by  $\Delta s$ . These values are used to populate the  $A$ ,  $B$ , and  $F$  matrices, which are sent to the MPC routine. The MPC routine calculates

**Table 1 Initial condition uncertainty parameters for dispersion analysis**

Initial condition	Mean	Standard deviation
Pitch angle ( $\theta$ )	0.1 rad	0.01 rad
Yaw angle ( $\psi$ )	0.0 rad	0.01 rad
Pitch rate ( $q$ )	-0.18 rad/s	2.0 rad/s
Yaw rate ( $r$ )	0.0 rad/s	2.0 rad/s
$x$ body velocity ( $u$ )	1143.3797 ft/s	15 ft/s
$y$ body velocity ( $v$ )	-0.00002502 ft/s	3 ft/s
$z$ body velocity ( $w$ )	0.375346 ft/s	3 ft/s

the optimal control sequence over the length of the update interval. When the projectile has covered the length of the first update interval, as well as every subsequent update interval, the controller is provided with full state feedback and the process is repeated. The control sequence calculated by the model predictive controller contains control inputs at increments of  $\Delta S$ . Linear interpolation is applied to determine control inputs between increments of  $\Delta S$ .

It is important to note that the controls resulting from the above calculations are expressed in the fixed plane frame, as per assumption number 1 in the Linear Theory section of this paper. To be applied to the canards, the control inputs must be converted to the conventional body fixed reference frame.

Each time Mach number is updated in the linear model, the matrices  $A$ ,  $B$ , and  $F$  are updated as well. This, in turn, requires updating of the gain matrices. The size of each of these matrices, and hence the computational time required to calculate them, is governed by the length of the prediction horizon. Obviously, frequent updates to the linear model and a long prediction horizon provide greater accuracy in the predictor and more efficient control. These observations are tempered with the need to limit the computational demand placed on the onboard processor.

**Results**

To establish the utility of the model predictive controller in a projectile application, a 4.5 ft long fin stabilized projectile is considered. The projectile has a total weight of 22.9748 lbf, a center of gravity location of 2.5 ft from the base, and four tail mounted stabilization fins. The roll and pitch inertias of the body are 0.0057 slug ft<sup>2</sup> and 1.35 slug ft<sup>2</sup>, respectively. A set of controllable canards, which alter the aerodynamic forces and moments, is located 4.25 ft from the base of the projectile.

To model uncertainty in launch conditions, which is a primary cause of dispersion, the initial pitch and yaw rates, pitch and yaw angles, and body velocities are all considered to be normally distributed random numbers with means and standard deviations that are representative of actual launch uncertainties. The values chosen are shown in Table 1.

The desired trajectory is chosen as that which the projectile would follow in the absence of uncertainty with initial conditions of  $x_0, y_0, z_0, \psi_0, \phi_0$ , and  $r_0=0, \theta_0=0.1$  rad,  $=1143.38$  ft/s,  $v_0 = -2.502 \times 10^{-5}$  ft/s,  $w_0=0.375$  ft/s,  $p_0=51.5$  rad/s, and  $q_0 = -0.18$  rad/s. The target location is chosen as  $x=6216.613$  ft,  $=0.261$  ft, and  $z=0.0$  ft. Figure 3 shows typical dispersion results for 50 sample trajectories with no control applied and initial condition perturbations as described above. The circular error probable (CEP) shown in the figure is based on a 50% hit criterion, that is, the CEP is defined as the minimum radius of a circle centered at the mean impact point and containing at least 50% of the shot impact points. With no control applied, the CEP is 106 ft. For reference, a second CEP is shown, which, instead of being centered at the mean impact point, is instead centered at the target location. A 50% hit criterion is still used. The second CEP has a radius of 113.5 ft.

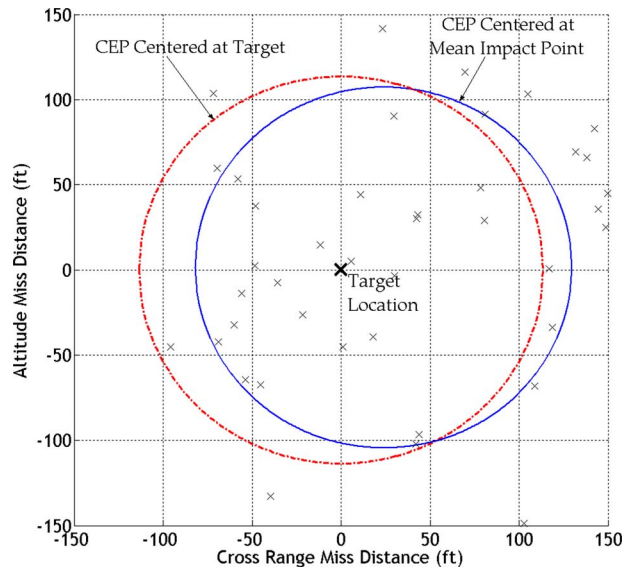


**Fig. 3 Uncontrolled dispersion (CEP=113.5 ft centered at mean impact point)**

Figure 4 shows the dispersion results with model predictive control applied. The prediction horizon,  $H_p$ , is chosen as 50. The error weighting matrix,  $Q$ , is chosen to be a function of range as follows:

$$Q = q \begin{bmatrix} \left(\frac{s_k}{1000}\right)^2 & 0 & 0 & 0 \\ 0 & \left(\frac{s_{k+1}}{1000}\right)^2 & 0 & 0 \\ 0 & 0 & \ddots & \vdots \\ 0 & 0 & \dots & \left(\frac{s_{k+H_p-1}}{1000}\right)^2 \end{bmatrix} \quad (47)$$

in which  $q$  is chosen, in this case, to be 0.5. By defining  $Q$  in this manner, the error weighting is increased quadratically as the projectile flies downrange. This prevents the tendency for the controller to attempt to force the projectile onto the desired trajectory

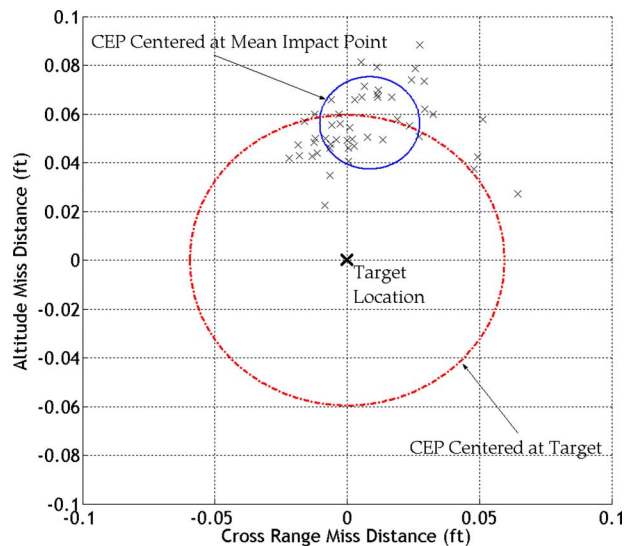


**Fig. 4 Controlled dispersion (CEP=0.02 ft centered at mean impact point)**

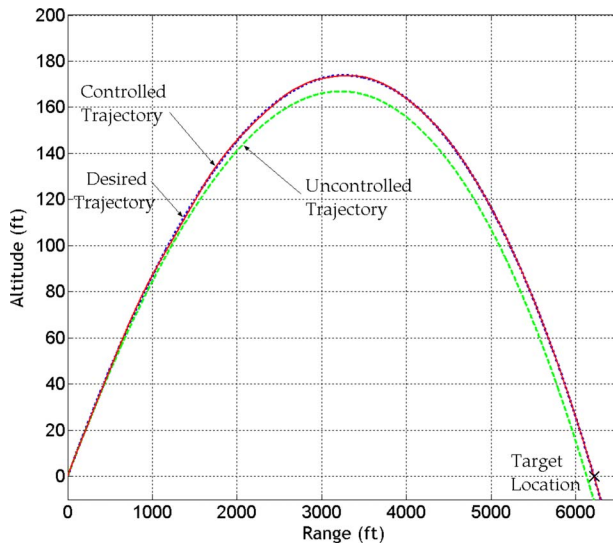


Fig. 5 Typical altitude versus range

immediately after launch, leading to a large initial control input followed by subsequent control inputs of nearly zero. In addition, the control weighting matrix,  $R$ , is defined to be

$$R = r \begin{bmatrix} H_p & 0 & 0 & 0 & 0 \\ 0 & H_p - 1 & 0 & 0 & 0 \\ 0 & 0 & \ddots & \vdots & \vdots \\ 0 & 0 & \dots & 2 & 0 \\ 0 & 0 & \dots & 0 & 1 \end{bmatrix} \quad (48)$$

where  $r$  is chosen as 2.0 in this case. By defining  $R$  in this manner, the current control value is weighted  $H_p$  times heavier than the control value at the end of the prediction horizon. This prevents large controls from being chosen at the beginning of an update interval, even if significant error is present. The model update interval for the case shown in Fig. 2 is 1000 arc lengths, and the arc length step size,  $\Delta s$ , is 20. These parameters provide a good baseline from which to begin examining the performance of the model predictive controller. Figures 5 and 6 show a typical con-

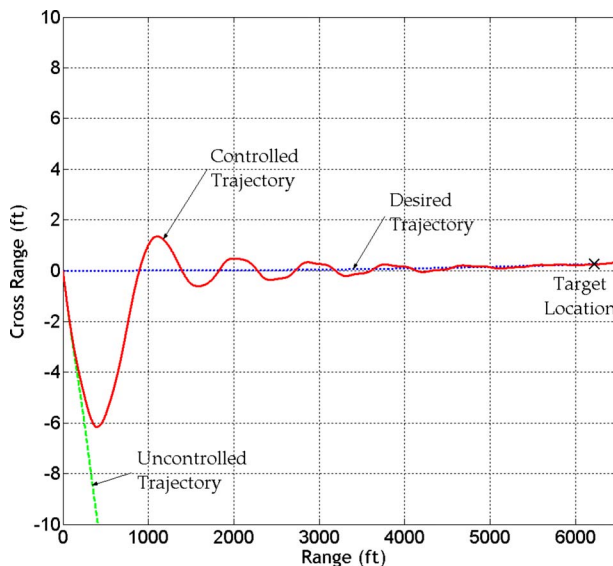


Fig. 6 Typical cross range versus range

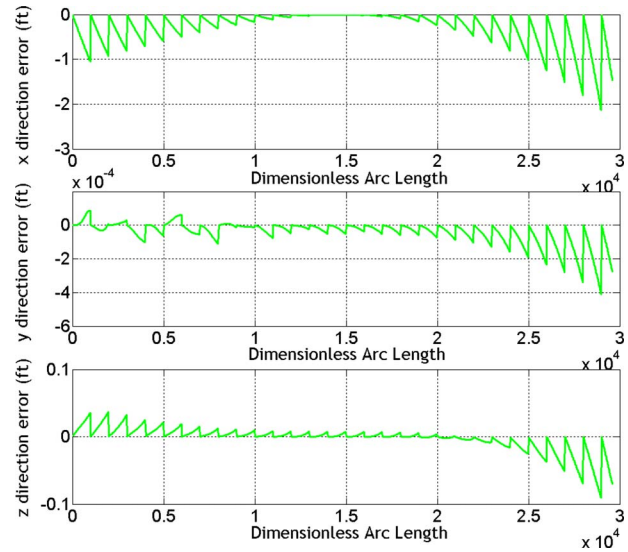


Fig. 7 Error between linear and nonlinear trajectory solutions

trolled and uncontrolled trajectory with the model predictive control parameters set as listed above.

The model predictive controller provides a very significant reduction in the CEP; from 106 ft in the uncontrolled case to 0.02 ft, or less than 1/4 of an inch, with control applied. It should also be noted that the mean impact point is almost 0.06 ft, or approximately 0.75 in., above the target location. In the cross-range direction, however, the mean impact point is only 0.0085 ft away from the target. This bias error in the  $z$ -direction can be attributed directly to errors in the linear model used in the predictor. One of the primary assumptions upon which projectile linear theory is based is that the projectile maintains a small angle of attack [25]. As the target is approached, the angle of attack of the projectile is forced to a small nonzero number. Though it is not necessarily in violation of the small angle of attack assumption, it is enough to cause a small deviation between the trajectory predicted with the linear model and that which is arrived at by integrating the full six degree of freedom nonlinear equations. This error is demonstrated by plotting the error between the validated, full, six degree of freedom, nonlinear trajectory, which is solved using a fixed step fourth order Runge–Kutta method, and the linear theory trajectory solution. The linear solution is corrected to match the nonlinear solution every 1000 arc lengths to mimic flight control system feedback. The control input is set equal to zero in both cases and the initial conditions are set to match those used in creating the desired trajectory. Figure 7 shows the linear theory error as a function of arc length in the  $x$ ,  $y$ , and  $z$  directions.

Note that the error is of the same order of magnitude near the end of the trajectory as the variation of the mean impact point in the CEP plot. It should also be noted that the error is greatest at the beginning and end of the flight, where the trajectory is furthest from horizontal. At the midpoint of the trajectory, where the path of flight is nearly flat and the projectile angle of attack is nearly zero, the error in all three spatial directions also becomes very close to zero.

Figure 8 shows the required control inputs for the trajectory shown in Figs. 3 and 4. The magnitudes of the control inputs required to achieve the shown degree of tracking are attainable for a set of nose-mounted canards.

Great care must be taken when choosing the gain values,  $q$  and  $r$ , such that the control values,  $C_{Y0}$  and  $C_{Z0}$ , never exceed approximately 1. Such large control inputs violate the small angle of attack assumption upon which the linearized model is based. As a result, the linear model no longer accurately approximates the true nonlinear system and the controller loses its ability to accurately

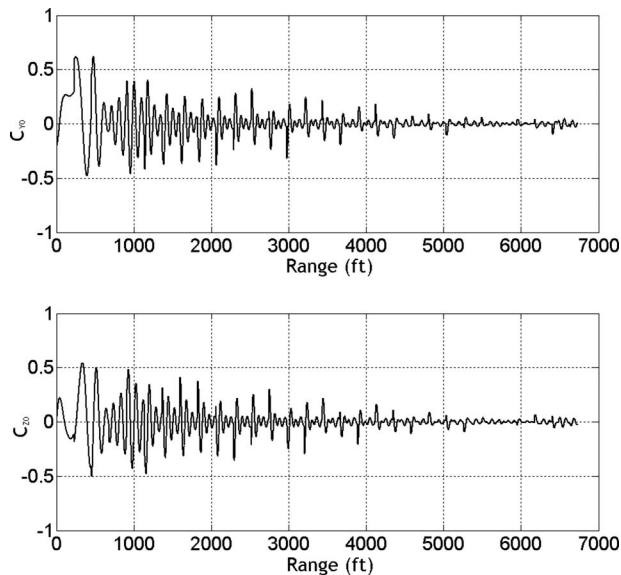


**Fig. 8 Required control inputs for a typical trajectory**

predict future states. When the system is provided with state feedback from the IMU under these circumstances, there are very large errors and the controller subsequently attempts to choose a large control value to compensate. Within one to two update intervals, the error becomes large enough that control saturates.

Other applications of model predictive control, such as that discussed by Mei et al.[2], use an iterative scheme to set a maximum control input value. In the application being discussed here, where speed of control computation is extremely critical, iteration is not practical. If the processor is occupied by an iterative routine while the projectile continues to fly downrange, control is lost. A second option is to simply clip the control values at the maximum allowable value. This, too, presents problems as future controls are calculated under the assumption that all previous controls were applied exactly as calculated.

The results discussed above assume perfect sensor feedback and precise knowledge of the mass and inertia properties of the projectile, both of which are unrealistic assumptions in real-world applications. In practice, sensors possess error created by both bias and noise, and manufacturing inconsistencies lead to slight mass and inertia property variations from one projectile to the next. The sensor inaccuracies are modeled in the simulation by choosing normally distributed random numbers with means of zero and standard deviations that are representative of commonly used IMU sensors. A bias value is randomly chosen for each sensor at the start of every flight simulation and retained throughout that particular simulation. In addition, a noise value is randomly chosen for each sensor every time feedback is implemented. Both the bias and noise value are added to the sensor readings at each update interval. The sensor bias and noise standard deviations used are summarized in Table 2. All subsequent results displayed

**Table 2 Sensor noise and bias values**

Sensor function	Bias standard deviation	Noise standard deviation
<i>x</i> and <i>y</i> positions	0.52 ft	0.52 ft
<i>z</i> position	1.18 ft	1.18 ft
<i>x</i> and <i>y</i> velocities	0.10 ft/s	0.08 ft/s
<i>z</i> velocity	0.16 ft/s	0.13 ft/s
Roll, pitch, and yaw angles	0.3 deg	0.3 deg
Roll, pitch, and yaw rates	0.05 deg/s	0.01 deg/s

in this paper employ sensor bias and noise applied in this way.

Additionally, manufacturing inconsistencies are modeled in the simulation by adding a normally distributed random number with a standard deviation of 1.5% of the nominal value to the variables representing projectile weight, inertia, and center of gravity locations. As would be the case in practice, the linear model, and hence the control system algorithm itself, operates using the nominal values.

Sensor noise and bias become the dominant sources of error when they are applied in this application. As the standard deviation of the sensor noise remains constant throughout the projectile flight, it no longer makes sense to define the error weighting matrix as a function of projectile range. Doing so, while keeping the value of  $q$  low enough to avoid violating the small angle of attack assumption near the end of the trajectory, unnecessarily limits the control action near the beginning of the trajectory. The error weighting matrix,  $Q$ , is instead defined simply as the identity matrix multiplied by the constant gain value,  $q$ .

Figure 9 shows dispersion results with mass and inertia property uncertainty and sensor noise and bias applied. The prediction horizon,  $H_p$ , is again 50. The error gain,  $q$ , is set to 1. The control weighting matrix,  $R$ , is defined as shown in Eq. (48) with the gain value,  $r$ , equal to 0.2. The update interval is 1000 arc lengths and the arc length step size,  $\Delta s$ , is 20. As a direct result of the mass and inertia property uncertainty and the sensor noise and bias, the CEP radius is increased to 1.9 ft. Removing mass and inertia property uncertainty, while leaving sensor noise and bias in place, leads to virtually the same result, indicating that the control system is not sensitive to small discrepancies in the linear model of the projectile.

To examine the stability of the discrete time linear model used in the control system, the eigenvalues of the system were examined over the length of the trajectory. This analysis was performed with both mass and inertia uncertainty and sensor and noise bias present, as well as with mass and inertia uncertainty removed. In both cases, the magnitude of the eigenvalues remained less than or equal to 1 over the entire trajectory, indicating a stable system.

In Fig. 10, the effects of changing both the control gain,  $r$ , and the prediction horizon,  $H_p$ , are shown. The model update interval is held constant at 1000 arc lengths and the arc length step size is held constant at 20 arc lengths throughout all of the simulations shown in Fig. 10. In addition, the error weighting matrix,  $Q$ , is defined as the identity matrix with the error gain,  $q$ , equal to 1. The control weighting matrix,  $R$ , is again defined as shown in Eq. (48). The control gain,  $r$ , is varied from 0.025 to 10 with the prediction horizon held constant. The process is repeated four times with values of  $H_p=25$ ,  $H_p=50$ ,  $H_p=75$ , and  $H_p=100$ .

As the value of  $r$  is increased, additional weight is given to the value of the control in the cost function (Eq. (43)). This in turn forces the magnitude of the chosen control values to be smaller, which provides less control authority. As would be expected, Fig. 10 shows that larger values of  $r$  lead to increased dispersion. However, there is a value of  $r$  below which the control values are allowed to be too large, leading to violation of the small angle of attack assumption and loss of control. This minimum value of  $r$  varies depending on the length of the prediction horizon. In Fig. 10, the lowest attempted values of  $r$ , which resulted in a controllable trajectory, are shown as the first data point for each series.

It is also apparent from Fig. 10 that, for a given value of  $r$ , there is a direct relationship between the length of the prediction horizon and the amount of impact point dispersion. Allowing the controller to take into account an increased number of the predicted states, as a longer prediction horizon does, leads to more intelligent control choices. It also significantly increases the amount of computation required at each update interval, necessitating a more expensive onboard processor.

A similar study was performed to investigate the effect of the length of the linear model update interval on the dispersion radius. The error weighting matrix,  $Q$ , is again the identity matrix with

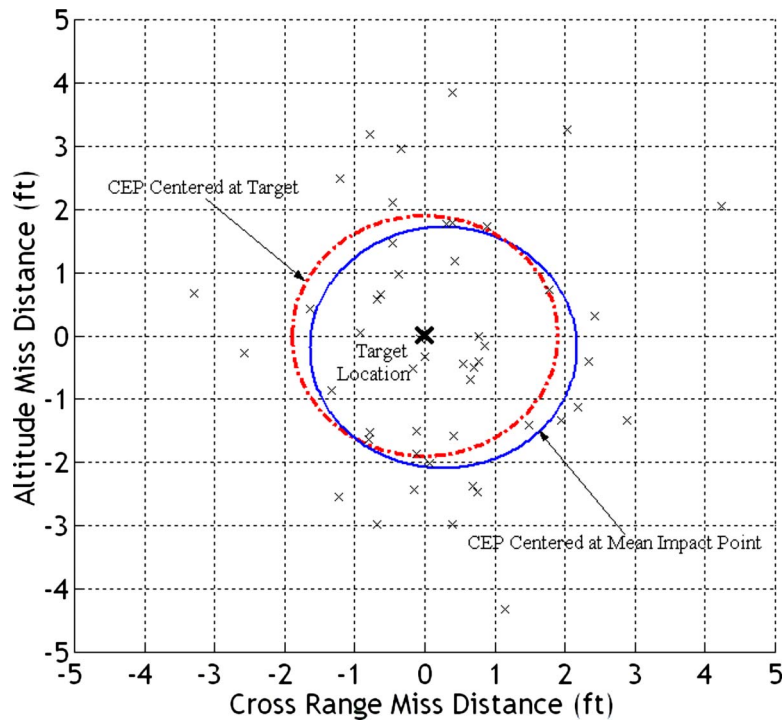


Fig. 9 Controlled dispersion with sensor bias and noise applied (CEP =2.1 ft centered at mean impact point)

the error gain,  $q$ , set to 1. The control weighting matrix,  $R$ , is defined as shown in Eq. (48) with the gain value,  $r$ , equal to 0.5. The arc length step size is again 20 arc lengths. The linear model update interval is varied from 100 to 2000 while holding the value of the prediction horizon constant. As before, the process is repeated four times with prediction horizon values of  $H_p=25$ ,  $H_p=50$ ,  $H_p=75$ , and  $H_p=100$ . The results are shown in Fig. 11.

Longer linear model update intervals lead to an increase in dispersion. This increase becomes more apparent for update intervals greater than 1000 arc lengths. For prediction horizon lengths of 25 and 50 arc length steps, update intervals greater than 1600 arc lengths led to a loss of control. This results from the linearized model deviating too far from the true nonlinear system. Upon

update, the error becomes very large and a large control is chosen to compensate, which in turn violates the small angle of attack assumption and causes further error in the linear model. Reducing the error gain,  $q$ , or increasing the control gain,  $r$ , would prevent this scenario from occurring. However, the tradeoff would be a reduction in control authority and an increase in dispersion.

The final study investigates the effects of the length of the step size,  $\Delta s$ , used by the controller to propagate the linear model forward. The prediction horizon is held constant at 50 steps and the error weighting matrix is the identity matrix with the gain,  $q$ , equal to 1. The control weighting matrix is defined, as shown in Eq. (48). Four values for the arc length step size ( $\Delta s=5$ ,  $\Delta s=10$ ,

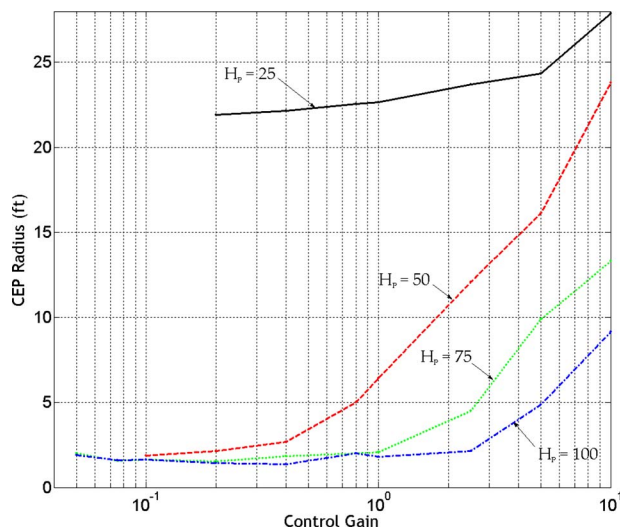


Fig. 10 Controlled dispersion results as the control gain,  $r$ , is varied

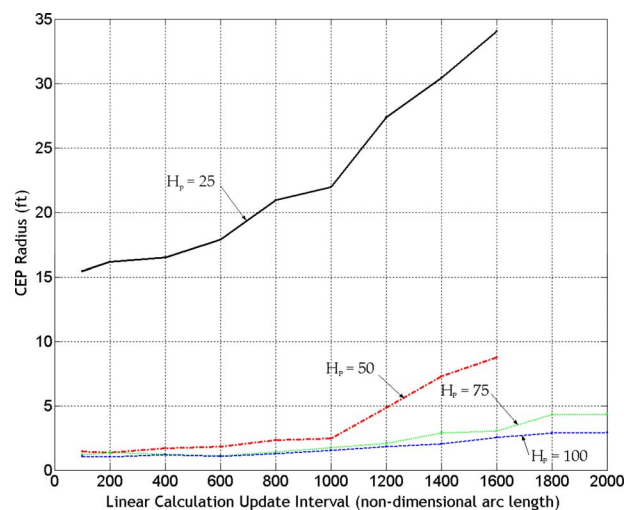
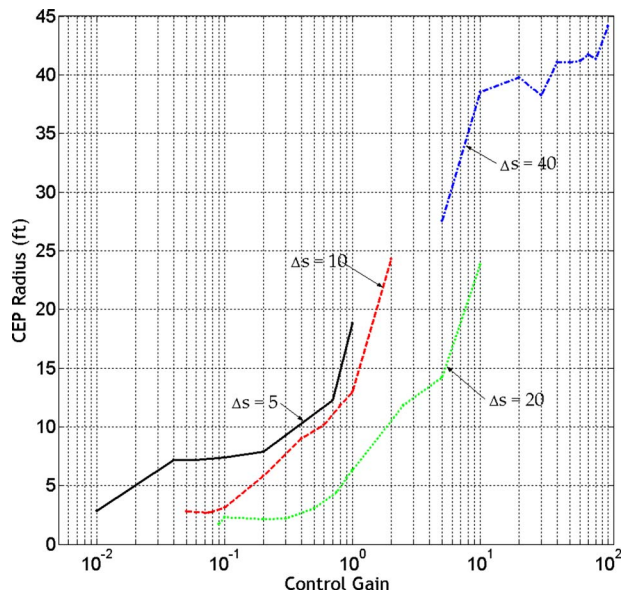


Fig. 11 Controlled dispersion results as the linear model update interval is varied



**Fig. 12 Controlled dispersion results as the arc length step size is varied**

$\Delta s=20$ , and  $\Delta s=40$ ) are used while the control gain,  $r$ , is varied over the range, which provided suitable control inputs for each step size. The results can be seen in Fig. 12.

As with any discrete linear model, the length of the step size has no effect on the accuracy of the model itself. However, as evidenced by Fig. 12, the length of the arc length step size does have an effect on the overall accuracy of the controller. This results from an interplay between two competing effects. The prediction horizon length is measured in the number of steps into the future that are used in the calculation of the optimal control. Therefore, for a given prediction horizon length, increasing the arc length step size allows the predictor to take into account state values farther into the future. However, control values are only calculated at each step increment, with control values between calculation steps derived from linear interpolation. A large step size can therefore lead to a decrease in resolution of the controller. For arc length step sizes of 5, 10, and 20, these effects do little more than change the acceptable range of gains, shifting the lines to the right of Fig. 12 for increasing values of  $\Delta s$ . However, at  $\Delta s=40$ , the controller becomes unable to provide the necessary amount of oscillation and dispersion is increased dramatically.

These parametric trade studies lead to a general set of guidelines for use in tuning an unconstrained model predictive controller in a projectile application. Arc length calculation step size, model update interval, and prediction horizon length all contribute to the amount of processing power required to run the control system in real time. The arc length step size should be as large as possible without losing controller precision. This study showed 20 arc lengths to be a good standard. Similarly, because of the large number of calculations required to create the control matrices, the model update interval should only be updated often enough to prevent the linear model from degrading too significantly. Previous study has shown the ideal value to be 1000 arc lengths and that value was confirmed here. Prediction horizons of 75 and 100 arc lengths provided only small improvements over a prediction horizon of 50 arc lengths, though reducing it to 25 arc lengths caused a dramatic loss of performance. A prediction horizon of 50 arc lengths would therefore be the minimum recommended value, though longer prediction horizons should be considered if the onboard processor is capable of handling the increased computational load. The control system gains should be the final consideration. As long as sensor noise proves to be the overriding source of error, the error weighting matrix should remain as the simple

identity matrix and, for simplicity, the error gain,  $q$ , can remain equal to 1. This leaves only the control gain,  $r$ , to be tuned for a specific projectile configuration. Through simulation,  $r$  should be chosen such that the control inputs avoid saturation, but control is not overly limited. In the case of the example projectile shown here, that value proved to be approximately 0.2.

## Conclusions

This paper develops a method for applying model predictive control, a proven and effective control technique, to a smart projectile application. The control law is shown to dramatically reduce the impact point dispersion caused by launch disturbances. The method uses full state feedback to create a linearized model of the projectile and quickly predict the future states of the system. These calculations can be performed by a relatively inexpensive onboard processor. As the predicted states depend on the states provided by the feedback loop, sensor accuracy is very important to the performance of the system and was shown here to be the limiting factor in dispersion reduction.

Considerable opportunities exist for the control system designer to tune the model predictive controller based on the desired application. It was shown that the length of the prediction horizon has a considerable effect on the dispersion radius, with a longer prediction horizon leading to a decrease in dispersion. However, a longer prediction horizon increases the size of the matrices used in the control calculation, which subsequently necessitates an increase in the processing power required to perform control calculations in a sufficiently short period of time. Shorter linear model update intervals lead to a decrease in dispersion as well, but with a similar increase in the amount of onboard computation required. The length of the arc length step size was shown to have little effect on dispersion as long as it remained below 20 arc lengths. Control and error gains should be adjusted to allow sufficient control authority without violating any of the assumptions upon which linear theory is based. No constraints are built into the controller to limit the size of the control inputs, so the control system designer should run a series of simulations prior to launching a projectile to ensure that the control and error gains are properly adjusted.

Though only a single direct fire projectile configuration was studied here, projectile linear theory can be applied to wide range of both direct and indirect fire projectiles, provided that they do not violate any of the assumptions detailed here in the section on Projectile Linear Theory. In addition, a few minor modifications can be made to the assumptions stated here, resulting in a related set of equations known as modified projectile linear theory, which allow a significant relaxation of the flat-fire assumption. With this in mind, model predictive control has the potential to be a powerful and widely applied control method in the smart munitions industry.

## Nomenclature

$\epsilon_{\text{curr}}$	= air density
$C_{NA}$	= normal force aerodynamic coefficient
$C_{MQ}$	= pitch rate damping moment aerodynamic coefficient
$C_{X0}$	= Aerodynamic drag coefficient in direction parallel to projectile motion
$C_{Y0}, C_{Z0}$	= aerodynamic trim coefficients perpendicular to projectile axis of symmetry
$C_{DD}$	= roll moment from fin cant
$C_{YPA}$	= magnus force
$C_{LP}$	= roll damping moment
$D$	= projectile characteristic diameter
$I_P, I_R$	= projectile precessional and rotational inertia
$m$	= projectile mass
$p, q, r$	= angular velocity vector components expressed in the body fixed reference frame

$\phi, \theta, \omega$  = Euler yaw, pitch, and roll angles  
 $\Delta SL$  = stationline distance from the projectile center of pressure location to the CG  
 $\Delta SL_M$  = stationline distance from the projectile Magnus force location to the CG  
 $\Delta SL_C$  = stationline distance from the control canard location to the CG  
 $u, v, w$  = translation velocity components of the projectile center of mass resolved in the body fixed reference frame  
 $x, y, z$  = position vector components of the projectile mass center expressed in the inertial reference frame  
 $V$  = magnitude of the mass center velocity  
 $L, M, N$  = total external applied moment on the rocket about the mass center expressed in the rocket reference frame  
 $X, Y, Z$  = total external applied force on the rocket expressed in the rocket reference frame  
 $H_p$  = prediction horizon used in model predictive controller  
 $s$  = dimensionless arc length

## References

- [1] Camacho, E., and Bordons, C., 1999, *Model Predictive Control*, Springer-Verlag, London.
- [2] Mei, G., Kareem, J., and Kantor, J., 2004, "Model Predictive Control of Wind-Excited Building: Benchmark Study," *J. Eng. Mech.*, **130**(4), pp. 459–465.
- [3] Tsai, C., and Huang, C., 2004, "Model Reference Adaptive Predictive Control for a Variable-Frequency Oil Cooling Machine," *IEEE Trans. Ind. Electron.*, **51**(2), pp. 330–339.
- [4] Kvaternik, R., Piatak, D., Nixon, M., Langston, C., Singleton, J., Bennett, R., and Brown, R., 2004, "An Experimental Evaluation of Generalized Predictive Control for Tiltrotor Aeroelastic Stability Augmentation in Airplane Mode of Flight," *J. Am. Helicopter Soc.*, **47**(3), pp. 198–208.
- [5] Slegers, N., and Costello, M., 2004, "Model Predictive Control of a Parafoil and Payload System," *Proceedings of the 2004 AIAA Atmospheric Flight Mechanics Conference*, Providence, RI, Paper No. 2004-4822.
- [6] Burchett, B., and Costello, M., 2002, "Model Predictive Lateral Pulse Jet Control of an Atmospheric Rocket," *J. Guid. Control Dyn.*, **25**(5), pp. 860–867.
- [7] Costello, M., and Anderson, D., 1996, "Effect of Internal Mass Unbalance on the Terminal Accuracy and Stability of a Projectile," *Proceedings of the 1996 AIAA Flight Mechanics Conference*, San Diego, C. A.
- [8] Murphy, C. H., 1980, "Symmetric Missile Dynamic Instabilities-A. Survey," *18th AIAA Aerospace Sciences Meeting*, Pasadena, CA, Jan. pp. 14–16.
- [9] Hodapp, A. E., 1976, "Effect of Mass Asymmetry on Ballistic Match of Projectiles," *J. Spacecr. Rockets*, **13**(12), pp. 757–760.
- [10] Weber, D. J., 1994, "Simplified Method for Evaluating the Flight Stability of Liquid-Filled Projectiles," *J. Spacecr. Rockets*, **31**(1), pp. 130–134.
- [11] Murphy, C. H., 1983, "Angular Motion of a Spinning Projectile With a Viscous Liquid Payload," *J. Guid. Control Dyn.*, **6**(4), pp. 280–286.
- [12] Cobb, K. K., Whyte, R. H., and Laird, P. K., 1983, "Effects of a Moving Components on the Motion of a 20-mm Projectile," *11th AIAA Aerodynamics Testing Conference*, Colorado Springs, CO, Mar. 18–20, pp. 94–103.
- [13] Hodapp, A. E., 1989, "Passive Means for Stabilizing Projectiles with Partially Restrained Internal Members," *J. Guid. Control Dyn.*, **12**(2), pp. 135–139.
- [14] Soper, W. G., 1978, "Projectile Instability Produced by Internal Friction," *AIAA J.*, **16**(1), pp. 8–11.
- [15] Costello, M., and Peterson, A., 2000, "Linear Theory of a Dual-Spin Projectile in Atmospheric Flight," *J. Guid. Control Dyn.*, **23**(5), pp. 789–797.
- [16] Murphy, C. H., 1981, "Instability of Controlled Projectiles in Ascending or Descending Flight," *J. Guid. Control*, **4**(1), pp. 66–69.
- [17] Cooper, G., 2001, "Influence of Yaw Cards on the Yaw Growth of Spin Stabilized Projectiles," *J. Aircr.*, **38**(2), pp. 266–270.
- [18] Guidos, B., and Cooper, G., 2000, "Closed Form Solution of Finned Projectile Motion Subjected to a Simple In-Flight Lateral Impulse," *38th AIAA Aerospace Sciences Meeting and Exhibit*, Reno, NV, Paper No. AIAA-2000-0767.
- [19] Burchett, B., Peterson, A., and Costello, M., 2002, "Prediction of Swerving Motion of a Dual-Spin Projectile With Lateral Pulse Jets in Atmospheric Flight," *Math. Comput. Modell.*, **35**(1–2), pp. 1–14.
- [20] Etkin, B., 1972, *Dynamics of Atmospheric Flight*, Wiley, New York, Chap. 4.
- [21] McCoy, R. L., 1999, *Modern Exterior Ballistics*, Schiffer Military History, Atglen, PA.
- [22] Murphy, C. H., 1963, "Free Flight Motion of Symmetric Missiles," U.S. Army Ballistic Research Laboratories, BRL Report No. 1216.
- [23] Cooper, G., and Costello, M., 2004, "Flight Dynamic Response of Spinning Projectiles to Lateral Impulsive Loads," *ASME J. Dyn. Syst., Meas., Control*, **126**, pp. 605–613.
- [24] Ikonen, E., and Kaddour, N., 2002, *Advanced Process Identification and Control*, Dekker, New York.
- [25] Costello, M., and Peterson, A., 2000, "Linear Theory of a Dual Spin Projectile in Atmospheric Flight," U.S. Army Research Laboratory, Technical Report No. CR-448.